Ceramics-Silikáty 67 (4), 477-485 (2023)
www.ceramics-silikaty.cz doi: 10.13168/cs.2023.0057

OSCILLATION OF THE GLASS FLOW IN A COLD-TOP ALL ELECTRIC MELTER

KENJI ODA*, YUJI TAJIMA**

*Institute of Glass Technology, J-1308, Shinano-cho 553-1, Totsuka-ku, Yokohama 244-0801, Japan
**ENO Suri Kaiseki Research, Katsushika-cho 2-371-1003, Funabashi, Chiba-pref. 273-0032, Japan

#E-mail: bach-ken@nifty.com, tajima@eno-research.co.jp

Submitted August 17, 2023; accepted November 18, 2023

Keywords: Glass flow, Cold-top, All electric melter, Internal Rayleigh number, Oscillation, Homogenisation

A three-dimensional unsteady mathematical model of thermal convection of glass melts was newly developed to investigate the oscillatory behaviour of glass flow in a cold-top all electric melter. A numerical simulation was performed to optimise the glass flow for the production of qualified glass, to examine the onset and transition of the thermal convection, and to demonstrate the effect of the pull and thermal properties on the oscillation. The numerical results verify the dependency of the oscillation mode on the internal Rayleigh number.

INTRODUCTION

Glass flow in a glass melting furnace plays an important role for batch melting, the redox and fining reaction, bubble transportation and homogenisation [1, 2, 3, 4].

The thermal convection of glass melts in a fuel-fired furnace (FFF) is driven by the density difference of the glass melts in a horizontal direction. The rough melt from the batch flows into the glass melts after the batch heating period. It is piled on the glass melts and stretched along the circulating flow for its dissolution [5]. A bubbler or stirrer agitates the glass melts to improve the homogeneity.

Numerous mathematical model studies have been devoted to simulating the steady glass flow in FFFs [6, 7, 8, 9, 10]. The quasi-stationary approximation of the batch log pattern is valid for intermittent batch feeding, reverse combustion and cyclic glass flow by a bubbler or stirrer. Agreement between the measurement and calculation confirms the information about the velocity and temperature of the glass melts, wall temperature, batch end line and velocity of the exhaust gas [11, 12].

The glass melting process in a cold-top all electric melter (AEM) is shown in Figure 1. It is affected by the humidity and pressure in the plenum, the ventilation of the decomposed gas through the batch, the tide of the foam, the heat flux from the glass melts to the batch through the foam layer, the unsteady glass flow and corrosion of the refractory or electrodes. Only a few research studies have been concerned with the numerical simulation of steady glass flow in AEMs [13, 14, 15, 16]. However, the oscillatory behaviour of the glass temperature can be observed in a vitrification melter [17]. There is no research into investigating unsteady glass flow in AEMs.

A new mathematical model of three-dimensional (3D) unsteady fluid flow coupled with Joule heating has been developed to solve the thermal convection of glass melts in AEMs. The numerical result presents time variant glass flow and elucidates on the periodicity of the oscillation.

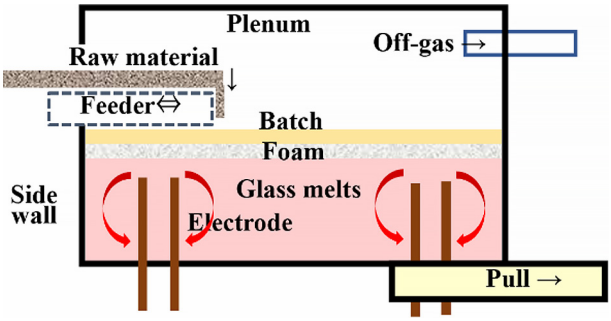

Figure 1. Schematic view of cold-top all electric melter.

THEORETICAL

Mathematical model

The following assumptions, I-IV, are made for glass melts.

I. It is incompressible and a Newtonian fluid,

II. Boussinesq approximation is applied,

III. Rosseland approximation is selected for the semi-transparency of glass melts, and

IV. Electrical conductivity is represented by the Rasch-Hinrichsen equation.

The 3D unsteady continuity, momentum and energy equations of the glass melts are described in Equations 1-3.

$$\nabla \cdot v = 0 \tag{1}$$

$$\rho_0 \partial v/\partial t + \rho_0 (\nabla \cdot v) v = -\nabla p + \mu \nabla^2 v + \rho_0 \boldsymbol{g} \beta (T - T_0) \tag{2}$$

$$\rho_0 c_p \partial T/\partial t + \rho_0 c_p (\nabla \cdot v) T = \nabla \cdot (\lambda \nabla T) + Q \tag{3}$$

where v, p, T and T_{ref} signify the velocity vector, pressure, temperature and reference temperature, respectively. Q is the Joule heat source per unit volume. ρ_0, c_p, μ, β, λ and g are the density, specific heat, viscosity, volumetric thermal expansion rate, thermal conductivity of the glass melts and acceleration due to gravity, respectively.

The furnace geometry and location of the electrodes for the numerical simulation are shown in Figure 2.

The inlet and outlet flow of the glass melts are assumed. The batch is heated by ascending glass melts from four corners, and the rough melt congregates in the central zone of the top surface of the glass. The inlet velocity is the batch melting rate, and the outlet flow corresponds to the throughput, called the pull.

A foam layer slips under the batch and the layer slides on the top surface of the glass. The other surrounding walls of the glass melts are non-slip in nature.

The thermal boundary conditions are assumed. The temperature of the top surface is fixed, and melting temperature of the rough melts is given as the inlet area. The heat flux on the side walls is supposed, and the bottom is thermally insulated.

The Joule heat distribution Q is obtained by solving Equations 4-6. Taking account of the connection, phase, location and configuration of the electrodes, the equation of voltage, V, is primarily solved. σ is the electrical conductivity of the glass melts.

$$\nabla \cdot (\sigma \nabla V) = 0 \tag{4}$$

As there is no significant difference between the solution of V at temperature dependent σ and that at constant σ [18], σ may be removed from Equation 4 to solve the V distribution.

The electrodes are firing diagonally across the melter, seen as the dashed line in Figure 2. The V distribution is solved for each pair of electrodes at a single phase without interference from the other 6 electrodes. It is supposed that the voltage of one electrode on the left back corner is E_0, and that on opposite corner is 0. All the surfaces surrounding the glass melts are electrically isolated.

In total, four V distributions are solved and superposed. The square of the gradient of the superposed V distribution is calculated, which is power coefficient P in Equation 5.

$$P = |\nabla V|^2 \tag{5}$$

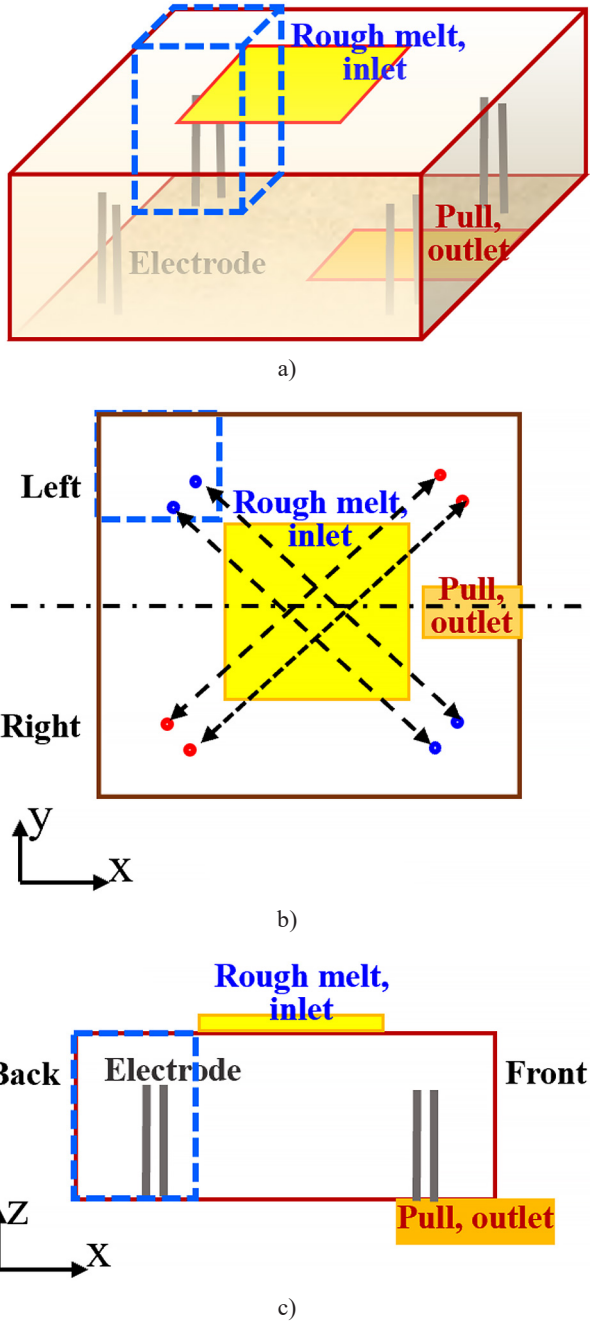

Figure 2. Glass flow domain and location of the electrodes: a) perspective, b) horizontal and c) vertical view.

The Joule heat Q is a product of P and the temperature dependent σ.

$$Q = \sigma P \tag{6}$$

where Q is adjusted so that the input power Q_e imposed on the glass melts is equal to $\int_G Q \, dG$, where G means the glass flow domain. Q is the heat source term in Equation 3.

Figure 3 shows the horizontal and vertical view of rectangle surrounded by dashed lines in Figure 2. The cross section of the electrode is square, and the electrodes are immersed in the bottom of the melter.

Numerical methods

The finite difference method is applied to solve Equations 1-6. The domain G, is divided into the cube of $\Delta x \Delta y \Delta z$. Momentum Equation 2 is discretised as Equations 7-9. A staggered grid is adopted for the discretisation [18]. The convective term of the energy Equation 3 is approximated by the 1st order upwind difference. The variable with "h" indicates the predicted variable at $t + \Delta t$.

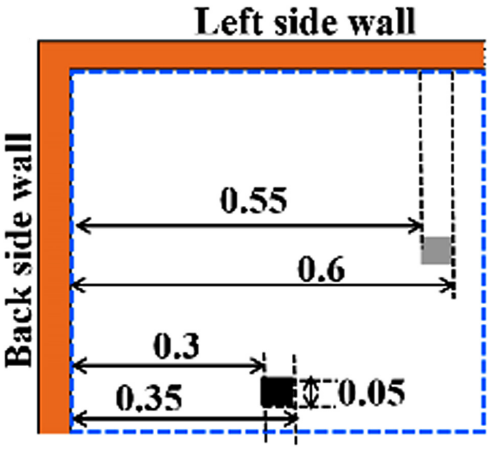

a)

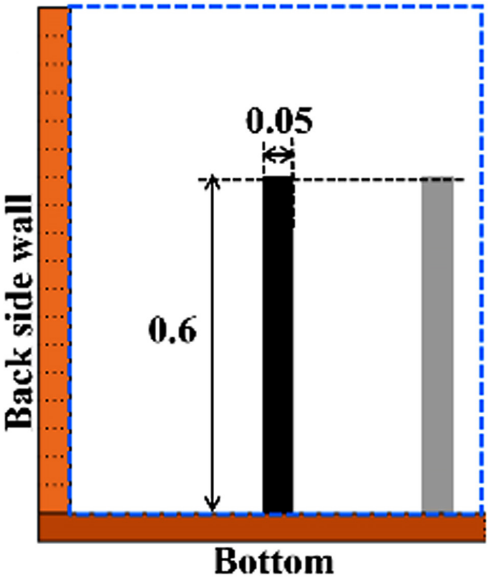

b)

Figure 3. Electrodes located in the left-back corner of Figure 2: a) horizontal and b) vertical view.

$$\rho_0 [(u^h_{i+1/2,j,k} - u_{i+1/2,j,k})/\Delta t + (u^2_{i+1,j,k} - u^2_{i,j,k})/\Delta x + \\ + \{(uv)_{i+1/2,j+1/2,k} - (uv)_{i+1/2,j-1/2,k}\}/\Delta y + \\ + \{(uw)_{i+1/2,j,k+1/2} - (uw)_{i+1/2,j,k+1/2}\}/\Delta z] = \\ = -(p_{i+1,j,k} - p_{i,j,k})/\Delta x + (\tau_{xx\ i+1,j,k} - \tau_{xx\ i,j,k})/\Delta x + \\ + (\tau_{xy\ i+1/2,j+1/2,k} - \tau_{xy\ i+1/2,j-1/2,k})/\Delta y + \\ + (\tau_{xz\ i+1/2,j,k+1/2} - \tau_{xz\ i+1/2,j,k-1/2})/\Delta z \tag{7}$$

$$\rho_0 [(v^h_{i,j+1/2,k} - v_{i+1/2,j,k})/\Delta t + \{(uv)_{i+1/2,j+1/2,k} - \\ - (uv)_{i-1/2,j+1/2,k}\}/\Delta x + (v^2_{i,j+1,k} - v^2_{i,j,k})/\Delta y + \\ + \{(vw)_{i,j+1/2,k+1/2} - (vw)_{i,j+1/2,k-1/2}\}/\Delta z] = \\ = -(p_{i,j+1,k} - p_{i,j,k})/\Delta y + (\tau_{xy\ i+1/2,j+1/2,k} - \tau_{xy\ i-1/2,j+1/2,k})/\Delta x + \\ + (\tau_{yy\ i,j+1,k} - \tau_{yy\ i,j,k})/\Delta y + (\tau_{yz\ i,j+1/2,k+1/2} - \tau_{yz\ i,j+1/2,k-1/2})/\Delta z \tag{8}$$

$$\rho_0 [(w^h_{i,j,k+1/2} - w_{i,j,k+1/2})/\Delta t + \{(uw)_{i+1/2,j,k+1/2} - \\ - (uw)_{i-1/2,j,k+1/2}\}/\Delta x + \{(vw)_{i,j+1/2,k+1/2} - (vw)_{i,j-1/2,k+1/2}\}/ \\ /\Delta y + (w^2_{i,j,k+1} - w^2_{i,j,k})/\Delta z] = -(p_{i,j,k+1} - p_{i,j,k})/\Delta z + \\ + (\tau_{xx\ i+1/2,j,k+1/2} - \tau_{xx\ i-1/2,j,k+1/2})/\Delta x + \\ + (\tau_{yz\ i,j+1/2,k+1/2} - \tau_{yz\ i,j-1/2,k+1/2})/\Delta y + (\tau_{zz\ i,j,k+1} - \tau_{yz\ i,j,k})/ \\ /\Delta z + \rho_0 g \beta (T_{i,j,k+1/2} - T_0) \tag{9}$$

where $u^2_{i,j,k}$, $(uv)_{i+1/2,j+1/2,k}$, $\tau_{xy\ i+1/2,j+1/2,k}$, etc. are approximated by the neighbouring velocity components.

$$\rho_0 c_p [(T^h_{i,j,k} - T_{i,j,k})/\Delta t + \{(u_{i+1/2,j,k} + |u_{i+1/2,j,k}|)T_{i,j,k} + \\ + (u_{i+1/2,j,k} - |u_{i+1/2,j,k}|)T_{i+1,j,k} - (u_{i-1/2,j,k} - |u_{i-1/2,j,k}|)T_{i,j,k} + \\ + (u_{i-1/2,j,k} + |u_{i-1/2,j,k}|)T_{i-1,j,k}\}/(2\Delta x) + \{(v_{i,j+1/2,k} + |v_{i,j+1/2,k}|) \\ T_{i,j,k} + (v_{i,j+1/2,k} - |v_{i,j+1/2,k}|)T_{i,j+1,k} - (v_{i,j-1/2,k} - |v_{i,j-1/2,k}|) \\ T_{i,j,k} + (v_{i,j-1/2,k} + |v_{i,j-1/2,k}|)T_{i,j-1,k}\}/(2\Delta y) + \{(w_{i,j,k+1/2} + \\ + |w_{i,j,k+1/2}|)T_{i,j,k} + (w_{i,j,k+1/2} - |w_{i,j,k+1/2}|)T_{i,j,k+1} - \\ - (w_{i,j,k-1/2} - |w_{i,j,k-1/2}|)T_{i,j,k} + (w_{i,j,k-1/2} + |w_{i,j,k-1/2}|)T_{i,j,k-1}\}/ \\ /(2\Delta z)] = \{\lambda_{i+1/2,j,k}(T_{i+1,j,k} - T_{i,j,k}) - \lambda_{i-1/2,j,k}(T_{i,j,k} - T_{i-1,j,k})\}/ \\ /(\Delta x)^2 + \{\lambda_{i,j+1/2,k}(T_{i,j+1,k} - T_{i,j,k}) - \lambda_{i,j-1/2,k}(T_{i,j,k} - T_{i,j-1,k})\}/ \\ /(\Delta y)^2 + \{\lambda_{i,j,k+1/2}(T_{i,j,k+1} - T_{i,j,k}) - \lambda_{i,j,k-1/2}(T_{i,j,k} - T_{i,j,k-1})\}/ \\ /(\Delta z)^2 + Q_{i,j,k} \tag{10}$$

where $\lambda_{i+1/2,j,k}$ is the average of the thermal conductivity of $T_{i+1,j,k}$ and that of $T_{i,j,k}$.

SIMPLE (semi-implicit method for pressure-linked equations) is adopted to solve the velocity and pressure [19]. The initial temperature of the glass is 1400 °C, and the velocity is 0 m·s^{-1}. The calculation starts from 0 s and is terminated at a t_{limit} of 172,800 s. The time increment Δt is 10 s to satisfy the Courant-Friedrichs-Lewy condition and the stability condition of Von Neumann. The whole numerical procedure is illustrated in Figure 4.

RESULTS AND DISCUSSION

The parameters for the calculation are listed in Table 1.

Length L, width W and depth D of G are 2.5, 2.5, 0.9 m, respectively. G is equally divided by a grid of

0.05 × 0.05 × 0.05 m^3 for the calculation. The inlet area is a 1.2 m square on glass top surface, and the outlet area is 0.5 m in length × 0.3 m in width rectangle on the bottom of the glass as shown in Figure 2.

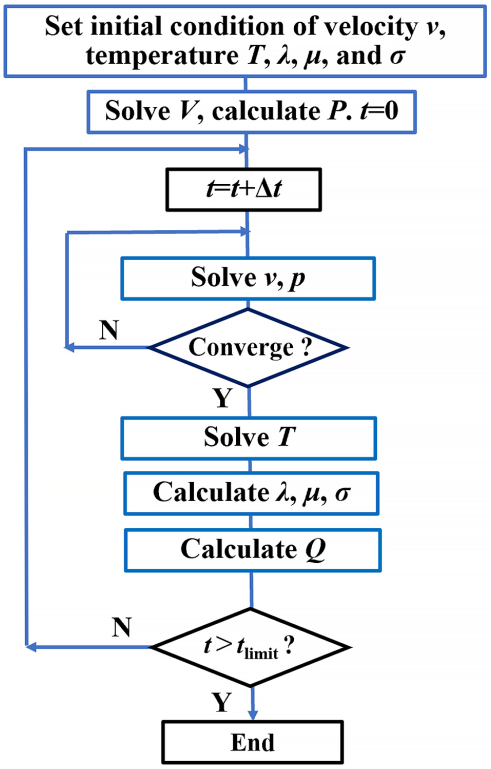

Figure 4. Numerical procedure.

The immersion length and cross section of the electrode are indicated in Table 1. Two electrodes are installed per corner. Each electrode centre is located 0.325 m from one sidewall and 0.575 m from the orthogonal wall, as shown in Figure 3. The temperature of the top surface of the glass is 800 °C, and the temperature of inlet area is 935 °C for the soda-lime-silicate (SLS) glass [20].

The thermal boundary conditions and physical properties of SLS glass melts are shown in Table 1. The input power Q_e of 2,000 kW is necessary for a pull of 10 t/d to attain the onset temperature of the fining, 1450 °C, to produce qualified glass, which are considered as the standard conditions (Std.) hereafter.

The internal Rayleigh number Ra_i is $\rho g \beta Q H^5/(\lambda a \mu)$. H is the characteristic length. Ra_i is a non-dimensional number to represent the status of the thermal convection in a cold-top and bottom heated cavity. It effects the oscillatory behaviour of the thermal convection.

Experiments were performed to measure the unsteady thermal convection of viscous glyceollin in a confined space without the inlet and outlet flow at room temperature [21, 22]. The results showed a fluctuation in the velocity or temperature of the liquid. It was seen in a cumulative study on the thermal convection in a cavity that a flow pattern below 10^7 at Ra_i shows periodic oscillation, and that the flow above 10^8 at Ra_i causes non-periodic time-dependent behaviour. Moreover, the previous research revealed periodic oscillation from 8.46×10^8 to 1.38×10^{10} at Ra_i [21].

Table 1. Parameters for the numerical simulation.

Geometry	Unit
Glass flow domain, L × W × D: 2.5 × 2.5 × 0.9	m^3
Inlet area: 1.2 × 1.2	m^2
Outlet area: 0.5 × 0.3	m^2
Electrode: 0.6 length × 0.05 square	m^3
Thermal boundary conditions	
Heat flux from the side wall: 2.0	kWh·(m^2 h)$^{-1}$
Heat flux from the bottom: 0.0	kWh·(m^2 h)$^{-1}$
Temperature of the inlet and the area: 935	°C
Temperature of the top surface of the glass: 800	°C
Physical properties of the glass melts	
Density, ρ_0: 2,300	kg·m^{-3} at 273 K
Specific heat, c_p: 1,300	J·(kg·K)$^{-1}$
Viscosity, log μ: –1.58 + 4332.0/(T – 248)	Pa·s at T °C
Thermal conductivity, λ: $-19.8 + 2.65\times10^{-8}\ T^3$	W·(m·K)$^{-1}$ at T K
Volumetric thermal expansion rate, β: 6×10^{-5}	K^{-1}
Electrical conductivity, σ: $953.0\times\exp(-5.56\times10^3/T)$	S·m^{-1} at T K

Ra_i of the glass flow in an AEM was reviewed with regards to the onset and periodic oscillation [23]. Ra_i is nominal for the glass flow, as the temperature dependent properties are distributed in the glass melts. When the characteristic length H is at depth D, Ra_i is 4.60×10^6 at 1000 °C and 6.84×10^7 at 1500 °C.

The cases for the simulation are listed from ① to ⑧ in Table 2. The internal Rayleigh number for ② – ⑧ may be described as $M\times Ra_i$. As the thermal diffusivity a is the thermal conductivity λ divided by the product of the density ρ and specific heat c_p, Ra_i is proportionate to $\beta/(\lambda^2\cdot\mu)$. Multiplier M reflects the ratio of the properties or Qe in ② – ⑧ to ①, and is shown in the rightmost column of Table 2.

The numerical simulation was performed to evaluate following issues, 1. – 4., from a viewpoint of Ra_i.

1. Glass flow for the melting and sulfate fining of the SLS glass,
2. Onset and transition of the thermal convection,
3. Dependency of the oscillation on noticeable properties, and
4. Attribution of the oscillation mode.

Table 2. Cases for simulation.

	Pull t/d	λ	μ	β	Q_e	M [–]
①	10	×1	×1	×1	×1	1
②	10	×1	×1	×1	×1/2	1/2
③	10	×1	×1	×1	×1/5	1/5
④	0	×1	×1	×1	×1	1
⑤	10	×1/2	×1	×1	×1	4
⑥	10	×1	×1	×1/2	×1	1/2
⑦	10	×1	×1/10	×1	×1	10
⑧	10	×1	×10	×1	×1	1/10

Glass flow for the melting and sulfate fining of the SLS glass

Case ① in Table 2 and the Std. in Table 1 are adopted to simulate the thermal convection of the SLS glass. The circulation of the glass melts is driven by both the buoyancy force and by the Joule heat and sensible heat of the pull. The flow pattern and temperature distribution on the *x*-*z* plane at 172,800 s are demonstrated in Figure 5 and Figure 6.

The glass flow ascends along the electrodes in Figure 5a and c, and descends on the centre plane in Figure 5b. The glass melts are heated near the side walls by electrodes as seen in Figure 6a and c, and the temperature is higher than the centre plane as seen in Figure 6b.

Figure 6 shows the flow pattern, Joule heat distribution and temperature distribution on the plane of $z = 0.6$ m. It can be observed from Figure 6a that the hot glass flows from the near front-right electrode to centre of the melter. As a result, the temperature distribution in Figure 5b (right) appears.

Figure 7 shows *T* and *w* at point A (1.25, 1.25, 0.85) beneath the batch. The initial velocity is 0 m/s and the temperature is 1400 °C. The glass temperature at point A beneath the batch is cooled by the descending flow of the

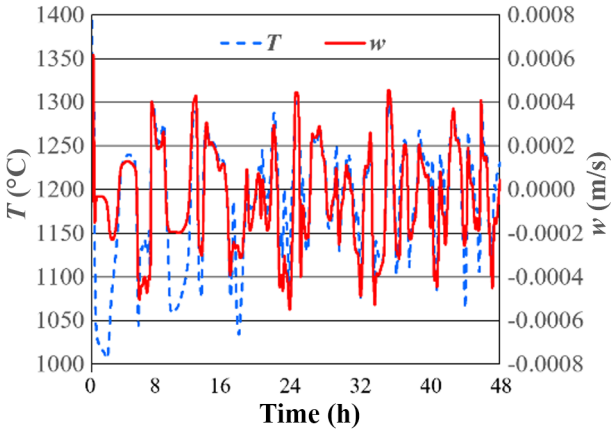

Figure 7. Variation in the T (blue dashed line) and w (red solid line) at point A with time from 0 to 48 h.

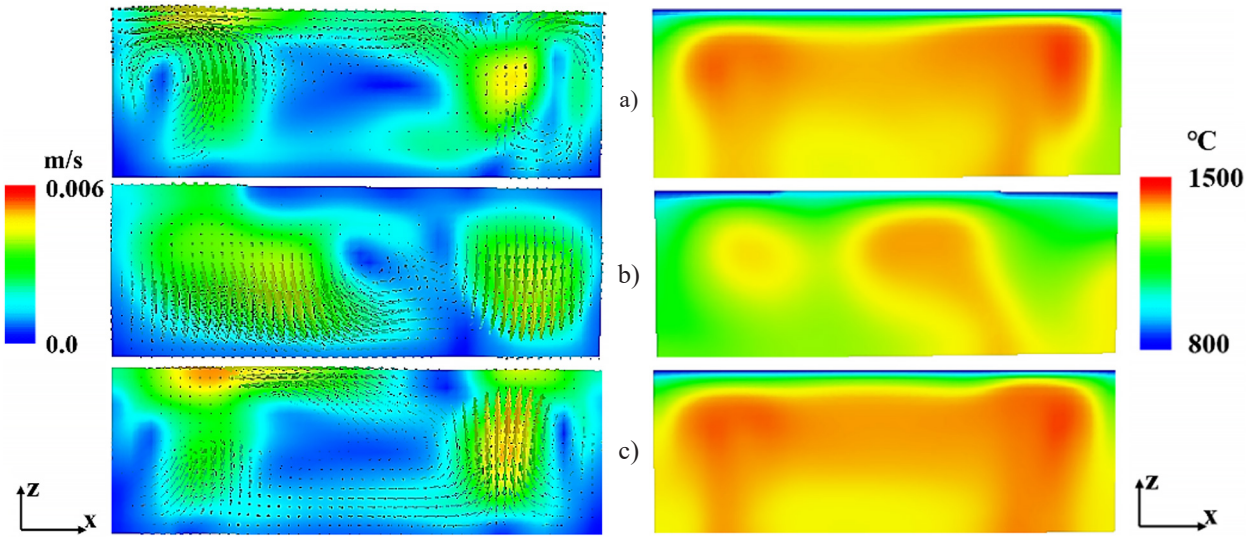

Figure 5. Velocity (left) and temperature (right) distribution on the plane of: a) y = 2.0 m, b) y = 1.25 m, c) y = 0.5 m at 48 h.

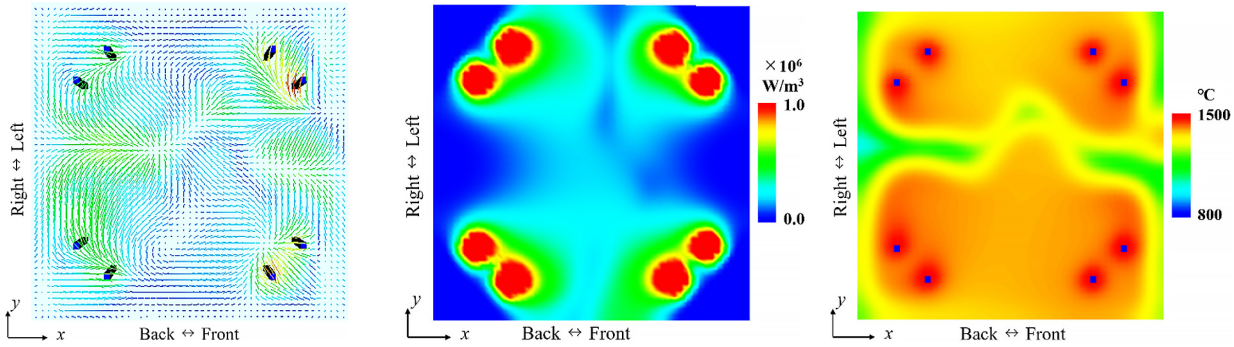

a) b) c)

Figure 6. Flow pattern a), Joule heat *Q* b) and *T* distribution c) on the plane of $z = 0.6$ m at 48 h.

inlet of 935 ℃. The temperature of point A is between 1400 ℃ and 935 ℃ during the transient process, and then the variable of the velocity or temperature attains periodical oscillation.

The oscillation is featured by both the frequency and amplitude of the velocity, $\boldsymbol{v}$ (u, v, w), and the temperature, T. There is a high correlation of T with w during the period from 4 h after the initial condition till 48 h, as the energy is transported by the sensible heat of the glass melts. w (A, t) may be the representative value of the oscillation, which is described as w hereafter, unless otherwise specified.

To produce a qualified glass product in the AEM, it is inevitable to keep the temperature zone higher than 1450 ℃ with regards to the oscillation.

Onset and transition of the thermal convection

The glass flow in the AEM is intrinsically unstable. There is no steady solution in the numerical simulation. The unsteady glass flow model is reliable in approaching steady state, to confirm the significance of the pull, and to predict the oscillation transition.

The effect of the Joule heating and pull on the oscillation of the glass flow is studied under following:

- Onset thermal convection of the glass melts,
- Acceleration of the oscillation by the pull, and
- Transition of the thermal convection.

Onset thermal convection of the glass melts

A Joule heat of 400 kW is imposed on the glass melts as in Table 2 ③.

Figure 8 shows the oscillation of w and T at point A beneath the batch, B (0.4, 0.4, 0.7) above the electrode, and C (2.25, 1.25, 0.05) above the outlet for a Q_e of 400 kW during the period from 8 to 48 h. w is quasi-steady at point A, but the velocity at point B or C fluctuates with the low frequency.

w (A, t) is slightly larger than the inlet velocity of 0.0000370 m/s, and it is quasi-steady as shown in Figure 8a. So, the mixing of the rough melt with the glass melts beneath the batch does not progress well. On the other hand, w(B, t) and w(C, t) are oscillating.

The sensible heat of the inlet at 935 ℃ is 136 kW, the Joule heat Q_e is 400 kW, and the total input energy is 536 kW. The total energy demand of the batch reaction is 174 kW [24], the heat loss from the side wall is 18 kW, the sensible heat of the outlet is 174 kW at 1200 ℃, and the total output energy is 366 kW. The residual energy of 170 kW is the radiation heat transport from the top surface of the batch to the plenum and the sensible heat of the decomposed gas. A Q_e of 400 kW is enough to induce thermal convection.

Acceleration of the oscillation by the pull

The glass flow for Table 2 ① and ④ is compared to confirm the effect of the pull. The results of w are presented in Figure 9.

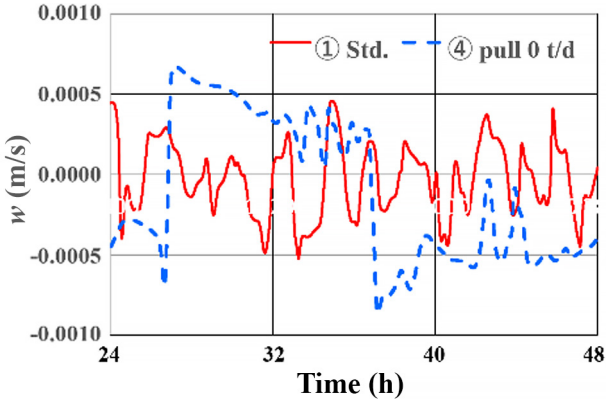

Figure 9. Variation in w with time from 24 to 48 h for the pull: ① Std. 10 (solid red line) and ④ pull 0 t/d (dashed blue line).

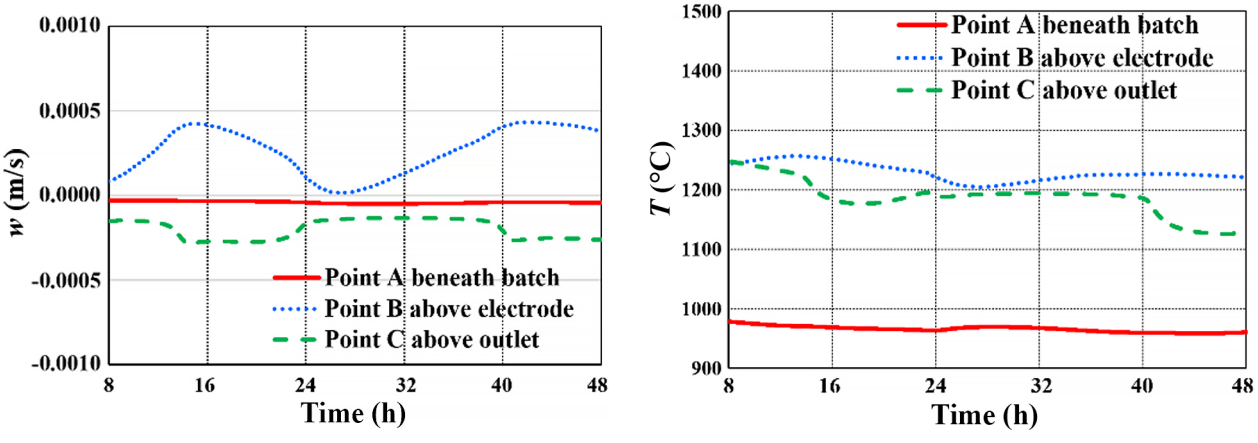

Figure 8. Variation in a) w and b) T with time from 8 to 48 h for a Q_e of 400 kW: point A (1.25, 1.25, 0.85), B (0.4, 0.4, 0.7) and C (2.25, 1.25, 0.05).

If the pull is 0 t/d, it takes about 20 hours for one oscillation cycle. It is easily seen that the inlet flow accelerates the oscillation and that the frequency of w is higher than without the inlet.

Transition of the thermal convection

The oscillation status is examined for Table 2 ① – ③. The viscosity of the glass melts varies with the temperature, and the temperature is controlled by the input power. To study the effect of the Joule heating, a simulation for a Q_e of 2000, 1000 and 400 kW was carried out.

Figure 10a shows the oscillation of w for a Q_e of 2000, 1000 and 400 kW during a term from 24 to 48 h.

If the Q_e increases and the viscosity decreases, w starts to oscillate. The amplitude at a Q_e of 1000 kW is smaller than 2000 kW, and the frequency at 1000 kW is lower than 2000 kW.

Figure 10b presents the maximum temperature T_{max} in the glass flow domain G at time t. If Q_e is not less than 2000 kW, the space for the onset fining temperature of 1450 °C is reserved.

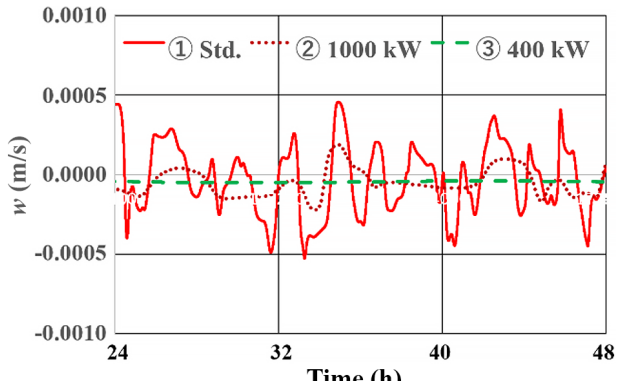

a)

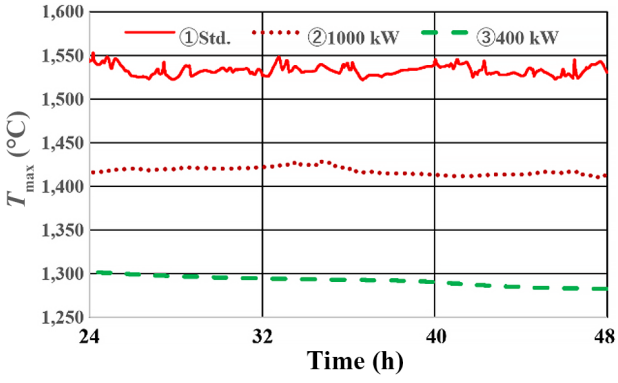

b)

Figure 10. Variation in the a) w and b) T_{max} with time from 24 to 48 h for Q_e: ① Std. 2000 kW (solid red line), ② 1000 kW (dotted brown line) and ③ 400 kW (dashed green line).

Dependency of the oscillation on the noticeable properties

The thermal conductivity of amber or tinted glass is smaller than the Std., and the volumetric thermal expansion rate of the neutral glass is lower than the Std. A simulation was carried out for Table 2 ⑤, ⑥, and the results are compared with the Std.

Figure 11 shows the oscillation of w for the glass of different properties at a Q_e of 2000 kW during the term from 24 to 48 h.

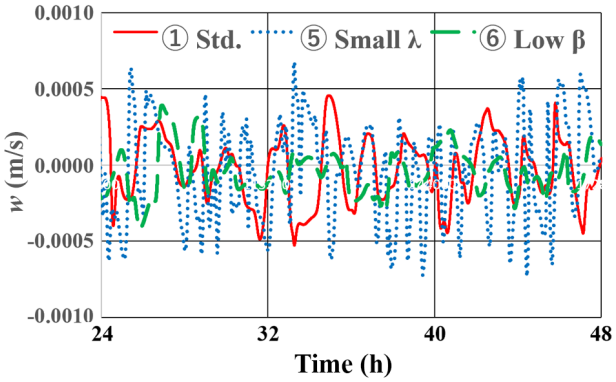

Figure 11. Variation in the w with time from 24 to 48 h for the properties: ① Std. (solid red line), ⑤ Small λ (dotted blue line) and ⑥ Low β (dashed green line).

It was found in Figure 11 that the amplitude of w for small λ glass is larger than the Std. or low β glass, and that the frequency is not lower than the others.

Figure 12 shows the variation in the maximum and minimum temperature T of the glass domain G with time for the Std., small λ and low β from 24 to 48 h. The solid or dashed line of each colour means the maximum or minimum temperature.

Multiplier M of ⑤ is larger than that of ①, which means the magnitude of the thermal convection of ⑤ is larger, too. The difference between the maximum and

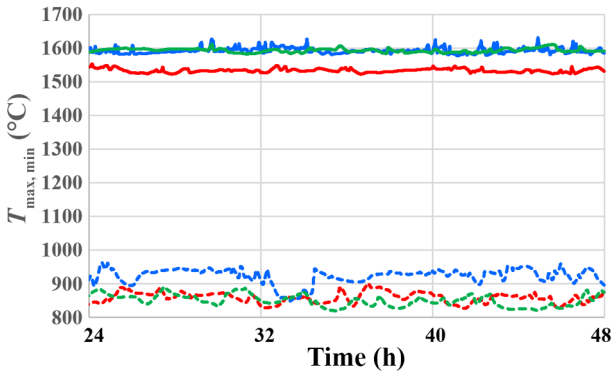

Figure 12. Variation in the maximum and minimum T with time from 24 to 48 h: ① Std. (red line), ⑤ Small λ (blue line) and ⑥ Low β (green line), where the solid and dashed line designate the maximum and the minimum.

minimum temperature of ⑤ becomes smaller than ①. On the other hand, the M of ⑥ is smaller than that of ①, and the difference becomes larger than ①. The Joule heat is concentrated near the electrodes in both cases of ⑤ and ⑥, and it is not easily transported to the surrounding glass. The maximum temperature of ⑤ and ⑥ is higher than ①.

Attribution of the oscillation mode

The viscosity of the glass wool is lower than the Std., and that of borosilicate glass is higher than the Std. A simulation was performed for Table 2 ⑦ and ⑧, and the results are compared with those for Table 2 ① and ②.

Figure 13 presents the variation in w for the glass of different kinds of viscosity at a Q_e of 2000 kW and a Joule heating Q_e of 1000 kW with time from 24 to 48 h.

The amplitude of w for the low viscosity glass is larger than the Std., the high viscosity glass or a Q_e of 1000 kW.

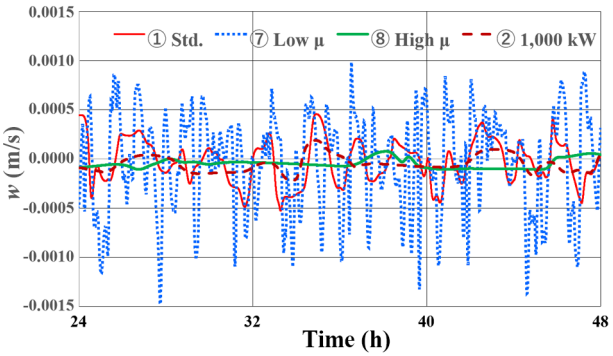

Figure 13. Variation in the w with time from 24 to 48 h

The numerical results give the maximum and the minimum of w as well as the number of dominant waves at point A during the term from 24 to 48 h. The amplitude of w is estimated as a half of their difference, and the cycle is the term of 24 h divided by the wave-number. Previous research [25] found that the cycle is proportionate to $Ra_i^{-2/3}$, which means that the cycle and $M^{-2/3}$ are in proportion, which are listed in Table 3.

Table 3. Oscillation mode for multiplier M.

M [-]	$M^{-2/3}$	Cycle (h)	Amplitude $\times 10^{-3}$ (m·s^{-1})	Acceleration $\times 10^{-3}$ m·s^{-2}
① 1	1.00	2.00	0.4880	0.06778
② 1/2	1.59	3.26	0.2020	0.01721
⑦ 10	0.22	0.80	1.2165	0.42240
⑧ 1/10	4.64	9.11	0.0925	0.00282

Figure 14 indicates that the numerical result coincides with the research. The amplitude exponentially decreases with $M^{-2/3}$.

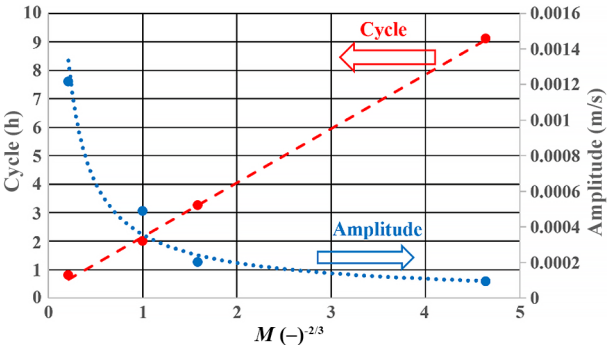

Figure 14. Variation in the Cycle (h) and Amplitude (m/s) at point A with M [-]$^{-2/3}$.

The homogenisation of the rough melt with the glass melts is enhanced by the oscillation of w, which allows the stretching and folding of Baker's transformation [26]. The stretching, folding and dispersion extend the molecular diffusion area. The oscillation accelerates the mixing, but it also fluctuates the glass quality. The compatibility of the homogenisation with the stability is measured by the acceleration, which is the amplitude divided by the cycle. The acceleration may be controlled by the Joule heating.

CONCLUSIONS

The numerical simulation of the 3D unsteady flow of the glass melts is carried out to clarify the oscillating behaviour of not only the velocity, but also the temperature in the AEM. The results verify the dependency of the oscillation mode of the glass flow on Ra_i.

Chaotic mixing is expected to accelerate the homogenisation of the glass melts in the AEM. It is indispensable to quantify the relationship of the oscillation mode with the variance in the glass quality. The comparison of the calculated temperature with the measured data in the AEM is required to validate the model. The global model of the glass flow, batch melting and tide of the foam will be evolved for the optimum design, operation, and control of the AEM.

REFERENCES

1. Oda K. (2022): Mathematical modelling of batch melting process in cold-top electric furnace. *Journal of the Ceramic Society of Japan, 130*(8), 701-706. doi: 10.2109/jcersj2.22068
2. Oda K., Kaminoyama M. (2009): Modeling of redox reaction in glass melt and its effect on glass flow. *Journal of Chemical Engineering of Japan*, *42*(11), 831-838. doi: 10.1252/jcej.08we261
3. Oda K., Kaminoyama M. (2009): Mathematical modeling sulfate fining in a glass melting furnace. *Journal of Chemical Engineering of Japan*, *42*, 868-877. doi: 10.1252/jcej.09we062

4. Oda K., Kaminoyama M. (2009): Mathematical model of bubble number density in glass tank furnace. *Journal of the Ceramic Society of Japan*, *117*(1366), 736-741. doi: 10.2109/jcersj2.117.736
5. Feng Z., Dongchun L., Guoqiang Q., Shimin L. (2008): Study of the float glass melting process: Combining fluid dynamics simulation and glass homogeneity inspection. *Journal of the American Ceramic Society*, *91*(10), 3229-3234, doi: 10.1111/j.1551-2916.2008.02606.x
6. Loch H., Krause D. (2002). Mathematical Simulation in Glass Technology, in Beerkens R. G. C. (Ed.): *Modeling of the Melting Process in Industrial Glass Furnaces*. Springer-Verlag. pp. 17-72.
7. Viskanta R. (1994): Review of three-dimensional mathematical modeling of glass melting. *Journal of Non-Crystalline Solids*, *177*, 347-362. doi: 10.1016/0022-3093(94)90549-5
8. Itoh H. (2002): Glass melting furnace and the simulation technology for its design and operation. *Journal of the Society of Inorganic Materials, Japan*, *9*, 327-332.
9. Schill P., Chmelar J. (2004): Use of computer flow dynamics in glass technology. *Journal of Non-Crystalline Solids*, *345/346*, 771-776. doi: 10.1016/j.jnoncrysol.2004.08.199
10. Oda K., Kaminoyama M. (2009): Method for evaluating thermal convection in molten glass flow in a glass tank furnace. *Journal of Chemical Engineering of Japan*, *42*(8), 555-562. doi: 10.1252/jcej.09we008
11. Mase H., Oda K. (1980): Mathematical model of glass tank furnace with batch melting process. *Journal of Non-Crystalline Solids*, *38/39*, 807-812. doi: 10.1016/0022-3093(80)90536-0
12. Wang J., Brewster B.S., McQuay M.Q., Webb B.W. (2000): Validation of an improved batch model in a coupled combustion space/melt tank/batch melting glass furnace simulation. *Glass science and technology (Frankfurt)*, *73*(10), 299-308.
13. Choudhary M.K. (1986): A three-dimensional mathematical model for flow and heat transfer in electrical glass furnaces. *IEEE Transactions on Industry applications*, (5), 912-921.
14. Igarashi H., Takahashi T. (1991): A three-dimensional mathematical model for an electric glass melter used to vitrify nuclear high level liquid waste. *Glass Technology*, *32*, 206-216.
15. Matsuno S., Iso Y., Uchida H., Oono I., Fukui T., Ooba T. (2008): CFD modeling coupled with electric field analysis for Joule-heated glass melter. *Journal of Power and Energy Systems*, *2*, 447-455. doi: 10.1299/jpes.2.447
16. Li H., Xing Z., Xu S., Liu, S. (2014): 3D simulation of borosilicate glass all-electric melting furnaces. *Journal of the American Ceramic Society*, *97*, 141-149. doi: 10.1111/jace.12597
17. Okubo T., Kanehira N. (2015): Establishment of vitrification technology in Rokkasho reprocessing plant. *Journal of Atomic Energy Society of Japan*, **57**, 511-516. doi: 10.3327/jaesjb.57.8_511
18. Mase H., Oda K., Takada A., Sato Y., Arai N., Kurata M. (1986): Three-dimensional mathematical model of glass tank furnace. *Journal of the Ceramic Society of Japan*, *94*, 285-294.
19. Patankar S.V., Spalding D.B. (1972): A calculation procedure for heat, mass and momentum transfer in three-dimensional parabolic flows. *International Journal of Heat and Mass Transfer*, *15*, 1787-1806.
20. Raether F., Krauss M. (2004): In-situ measurements of batch glass during melting. *Glass science and technology (Frankfurt)*, *77*(3), 118-123.
21. Kawaguchi T., Saito T., Satoh I. (2012): Experimental analysis of natural convection with Joule heating by means of particle image velocimetry. *16th Int. Symp. on Applications of Laser Techniques to Fluid Mechanics*.
22. Zhou J., Takahashi H., Tsuzuki N., Kikura H. (2018): Investigation of flow behavior of Joule-heating flow in a 2-D model of a reprocessing glass melter cavity. *Journal of Flow Control, Measurement & Visualization*, *6*, 199-216. doi: 10.4236/jfcmv.2018.64016
23. Smrček J. (2007): Significance of Rayleigh number for all-electric melting. *9th International Seminar Mathematical Modeling of Furnace Design and Operation*.
24. Verheijen O.S. (2003). *Thermal and chemical behavior of glass forming batch*. Technische Universtiteit Eindhoven. doi: 10.6100/IR565202
25. Busse F.H., Whitehead J.A. (1974): Oscillatory and collective instabilities in large Prandtl number convection. *Journal of Fluid Mechanics*, *66*(1), 67-79. doi: 10.1017/S0022112074000061
26. Ottino J.M. (1989). *The kinematics of mixing: stretching, chaos, and transport*. Cambridge University Press.